RSC Advances

ROYAL SOCIETY OF CHEMISTRY

www.rsc.org/advances

RSC Advances

RSCPublishing

COMMUNICATION

Fe Whisker Growth Revisited: Effect of Au Catalysis for [02$\bar{1}$] Oriented Nanowires with 100-nm Diameter

Cite this: DOI: 10.1039/xoxxoooooox

T. Yanase,[a] A. Kawahito,[b] Y. Hashimoto,[b] T. Endo,[c] Y. Wang,[d] T. Nagahama[e] and T. Shimada[e,f]

Received ooth January 2012,
Accepted ooth January 2012

DOI: 10.1039/xoxxoooooox

www.rsc.org/

We re-examined the growth of single crystalline Fe whiskers by chemical vapour deposition with regard to modern nanowire (NW) growth techniques. Single Fe NWs (100 – 300 nm diameter) with a high aspect ratio and unique [02$\bar{1}$] orientation were grown by optimizing the flow of raw materials ($FeCl_2$ and H_2) and using a Au nanoparticle catalysis and single crystalline substrate. The growth mechanism was investigated by transmission electron microscopy and electron diffraction analysis of the NW-catalysis interface.

Introduction

Single crystalline whiskers of Fe have been synthesized by the simple reduction of $FeCl_2$ in a H_2 atmosphere without a gas flow in the 1960s – 1970s[1-3] and used to study the dynamics of magnetic domains[4]. However, Fe whiskers grown via the gas phase have almost been forgotten in the recent research trends of single crystalline nanowires (NWs) grown by chemical vapour deposition (CVD) techniques. This is because the diameter of the Fe whiskers grown by conventional CVD techniques is very large (several μm) and the orientation of the NWs could not be precisely controlled. In addition, the CVD used in 1960s – 1970s for fabrication of Fe whiskers is now outdated because the Fe whiskers can only be grown on $FeCl_2$ powders by simple reduction in the crucible. Furthermore, the simple CVD system makes it impossible to precisely control the growth conditions.

Nevertheless, magnetic NWs, including Fe NWs, have been studied by many researchers due to not only their unique magnetic anisotropy but also to their potential for applications, such as a precursor of permanent magnets, spintronic devices, sensors, etc[5-8]. Although some research on the fabrication of Fe NWs by alternating current electrodeposition has been reported, NWs fabricated by electrodeposition are basically polycrystalline[9-11]. Large number of steps, including fabrication of alumina oxide (AAO) template, electrodeposition, and AAO removal, to yield the freestanding Fe NWs by electrodeposition method is another disadvantage. Nanoimprint-lithography is another technique to fabricate Fe NWs[12], however, single crystalline NWs cannot be fabricated due to the use of epitaxial growth and subsequent etching process, resulting principally in polycrystalline NWs. The necessity of large equipment and unsuitability for large scale production are also disadvantage of nanoimprint-lithography.

Since the crystallinity of NWs strongly affects their magnetic properties[13], NWs should be single crystals. CVD is one of the best techniques to easily obtain single crystal NWs. Another advantage of CVD is to economically fabricate NWs in large quantity, which could realize various NW applications. The fabrication of Fe NWs (whiskers) has not been studied since the 1970s, yet the synthesis of Fe NWs using CVD techniques has become realistic because many kinds of NWs have been intensively investigated by CVD techniques for years[14-20]. In particular, it is well-known that the catalyst and substrate significantly affect the morphology of the NWs. Furthermore, the core-shell structure, which was recently studied due to its possibility for new applications, such as spin valve devices, drug delivery, and passivation of the NW surface, can be easily fabricated if CVD techniques to fabricate Fe NWs are established[21-23].

In this paper, we report the effect of Au nanoparticle catalysis, substrate, and orientation of the substrate. The growth mechanism will be discussed by investigating the morphology, crystal structure, and orientation of the NWs.

Experimental

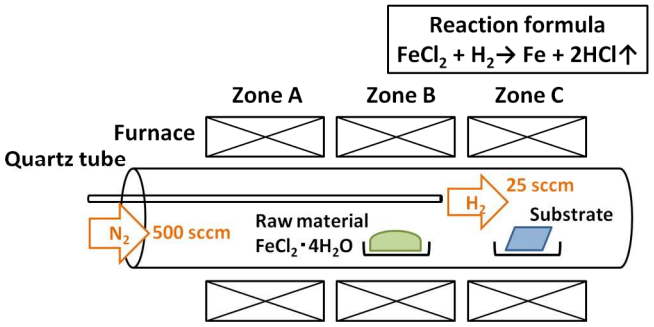

Fig. 1 Schematic illustration of CVD with gas flow separation system for controllable fabrication of Fe NWs.

Figure 1 shows the CVD system to grow Fe NWs in this study. The furnace has three temperature-controllable zones which are labelled from upstream zone A, zone B, and zone C. $FeCl_2 \cdot 4H_2O$ (purchased from Kanto Chemical Co., Inc.) without any further purification and substrates were installed in zone B and zone C, respectively. Si and Al_2O_3 were chosen as the substrate. The Si substrates were cleaned by the Radio Corporation of America cleaning method to remove any metal and organic contaminations on the surface[24]. The Al_2O_3 substrates were annealed at 1000 ºC for 5 hours to clean the surface before placing in the quartz tube. After the substrate were cleaned by these methods, Au nanoparticles (average diameter = 30 nm) dispersed in a citrate solution were spin-coated on the substrate. Au nanoparticles suspension was prepared by the same method in Ref. 25. Subsequently, the substrates were annealed at 300 ºC for 30 min in an ambient atmosphere to remove the citric acid from the surface of the Au nanoparticles[25], and then the substrates were placed in the quartz tube. Since Fe can partially dissolve in Au[26], it was expected that the Au nanoparticle is a good catalyst, and the Fe NWs grow by the vapour-liquid-solid (VLS) or vapour-solid (VS) mechanism[17,27]. The schematic illustrations of VLS and VS mechanism are shown in supplementary information (scheme S1). The distance between the $FeCl_2 \cdot 4H_2O$ and the substrates was approximately 8 cm. The flow paths of the reaction gas (3.9% H_2 + 96.1% Ar) and carrier gas (99.99% N_2) are separated from upstream to zone B. H_2 gas flowed through the inner quartz tube with the inner diameter of 4.0 mm, and the carrier gas with $FeCl_2$ vapour flowed through the outer quartz tube with the inner diameter of 37.5 mm. These two gases were mixed at the end of zone B. $FeCl_2$ and H_2 molecules in the vapour phase diffuse to the surface of the substrates and the CVD proceeded. The separation of the gas flow path hinders the reduction of the $FeCl_2$ powder in zone A, which enables a continuous supply of clean $FeCl_2$ vapour. This flow separation system is crucial methodology to synthesize the Fe NWs with a good repeatability and control.

The N_2 flow started at the flow rate of 500 sccm after the $FeCl_2 \cdot 4H_2O$ and the substrates were installed in the quartz tube. H_2 gas was not introduced when the N_2 flow started in the early stage. The $FeCl_2 \cdot 4H_2O$ was heated at 200 ºC for 30 min to remove the crystal water before the CVD was carried out. After removal of the crystal water from the $FeCl_2 \cdot 4H_2O$, each zone of furnace was heated to a preset temperature within 2 – 3 hours. The temperatures of zone A and zone B was 550 ºC and 600 ºC, respectively, while the temperature of zone C was ranged from 600 ºC to 920 ºC as the growth condition parameter. When the temperatures of all the zones were attained at the preset temperatures, the H_2 flow started at the flow rate of 25 sccm. The reaction was continued for 5 – 30 min then the H_2 flow was immediately cut off after the desired reaction time was reached. The furnace was subsequently cooled to room temperature while maintaining the N_2 flow.

The morphology of the Fe NWs was observed by scanning electron microscopy (SEM; JEOL JSM-6500F and JSM-6390LVS). The crystallinity and growth axis of the Fe NW were investigated by X-ray diffraction (XRD; Rigaku RINT2200) and transmission electron microscopy (TEM; JEOL JEM-2010). An energy dispersive X-ray spectrometer (EDS) equipped with SEM was used for the elemental analysis.

Results and discussion

Figure 2 shows SEM images of the surface of the Al_2O_3 substrate (0001) (C-plane) (a) with Au nanoparticles and (b) without Au nanoparticles after the CVD was carried out. Not only particles, but also a large number of NWs were observed on the Al_2O_3 substrates with Au nanoparticles while there are only prism-shaped particles on that without the Au nanoparticles. The growth temperature and the growth time were 700 ºC and 30 min, respectively. NWs can be grown only at temperatures between 600 ºC and 850 ºC. At temperatures lower than 600 ºC, only particles were formed on the substrate even though the Au nanoparticles were spin-coated on the substrates. This is because the reduction reaction proceeds very slowly at such a low temperature. At temperatures higher than 850 ºC, the substrates were completely covered by a thin polycrystalline Fe film because the reduction reaction proceeds very rapidly, which means no selective growth at such high temperatures. These results indicate that the Au nanoparticles acted as catalysts to grow the Fe NWs, and the growth temperature must be precisely controlled. It was found that the diameter of the NWs (100 – 300 nm) was much larger than the size of the Au nanoparticles (30 nm), which implies that the diameter of the Fe NWs was determined by other factors. The average aspect ratio of the Fe NWs on the Al_2O_3 substrate was approximately 45. Although Si substrates spin-coated with Au nanoparticles were also attempted, no Fe NW was formed, which implies that the choice of the substrate was also important (see Fig. S1 in supplementary information).

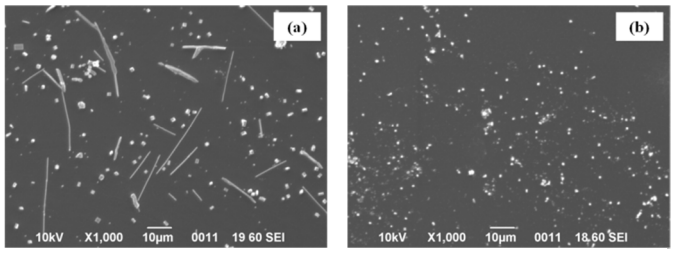

Fig. 2 Surface morphologies after CVD was carried out at 700 ºC for 30 min (a) with Au nanoparticles and (b) without Au nanoparticles.

The NWs were examined by XRD and EDS as shown in Figs. 3(a) and 3(b). The NWs were grown at 700 ºC for 30 min on C-plane Al_2O_3 substrates. In the XRD pattern, there are three main peaks which can be assigned to α-Fe 110, 200, and 112. No iron compound, such as Fe_2O_3 and $FeCl_2$, was observed, which shows that $FeCl_2$ was completely reduced by H_2, and the surface of the Fe NWs was not oxidized within several hours in air. EDS mapping also showed that the NWs were composed of Fe, and no other element was detected in the NWs, which supports the results of the XRD analysis. In addition, an elemental depth profile of the Fe NW stored in air for 3 days was obtained by Ar etching in the XPS analysis to investigate the oxidation tolerance that is important for application (see Fig. S2 in supplementary information). Fe^{3+} was observed on the surface of the NWs. The intensity of Fe^{3+} decreased as the NW was etched deeper into the inside while the intensity of Fe^0 increased. This result proves only several nm from the surface of the NW was oxidized and Fe

completely remained inside. The oxidized Fe at the surface works as the passive state and hinders more oxidation.

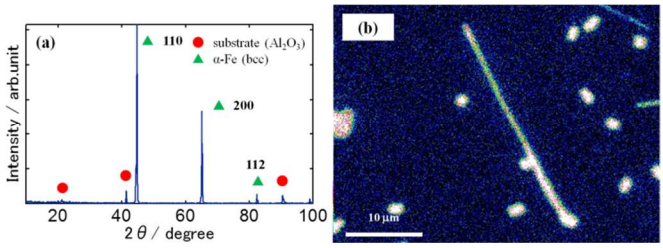

Fig. 3 (a) XRD pattern and (b) Fe mapping by EDS of Fe NW grown at 700 ºC for 30 min with Au nanoparticles.

Based on the SEM observations, we noticed many NWs with a greater aspect ratio were seen on the edge of the C-plane Al_2O_3 substrate (see Fig. S3 in supplementary information). This clearly indicated that the growth rate of the Fe NWs depends on the orientation of the substrate. The M-plane Al_2O_3 substrate, which is perpendicular to the C-plane, was used to improve the aspect ratio of the Fe NWs. Figures 4(a) and 4(b) show that the aspect ratio of the NWs grown on the M-plane Al_2O_3 (approximately 300) is greater than that on the C-plane Al_2O_3. An expanded figure of the Fe NW is shown in Fig. 4(b) as an inset.

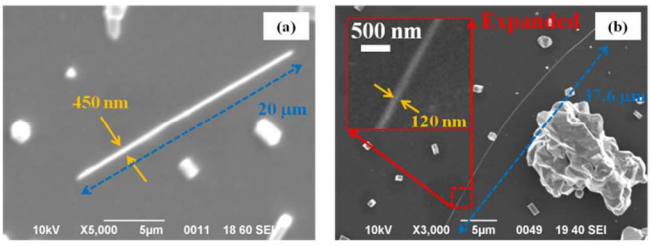

Fig. 4 Comparison of the aspect ratio of the Fe NWs grown at 700 ºC for 30 min on (a) C-plane Al_2O_3 (b) M-plane Al_2O_3.

The early stage of the NW growth was observed to understand the growth mechanism of the Fe NWs in detail. Figure 5 shows the Fe NW grown at 700 ºC for 5 min on the M-plane Al_2O_3 substrate with Au nanoparticles. The Au nanoparticles aggregated and became island-like structures (called a Au island below) because nanoparticles tend to minimize the surface energy[28]. The NW growth started at one point on the surface of a Au island as shown in Fig. 5 by the circle. The NW grew in two directions from the starting point and the growth direction was horizontal to the substrate. As seen in Fig. 5, there is no Au particle at the tip of the NW. This illustrates that the growth mechanism of Fe NWs is the self-catalytic VS mechanism, not the VLS mechanism. Secondly, the Fe NWs grown at 700 ºC for 30 min on the M-plane Al_2O_3 substrates were investigated. No Au nanoparticles could be found on the surface of the substrate in an SEM image and no Au was detected in the EDS and XPS (not shown here). To confirm the location of Au, a cross section at the centre of the NW was observed by TEM as shown in Fig. 6(a). It was found that there was a thin Au layer (~20 nm) between the NW and the substrate, which means that the Au islands after aggregation were covered by Fe if the reaction time is long enough. This is why Au was not detected by EDS and XPS. Note that the NW was connected to the Au layer, which indicates that the NW growth started from the surface of the Au island. This result is consistent with the SEM observations.

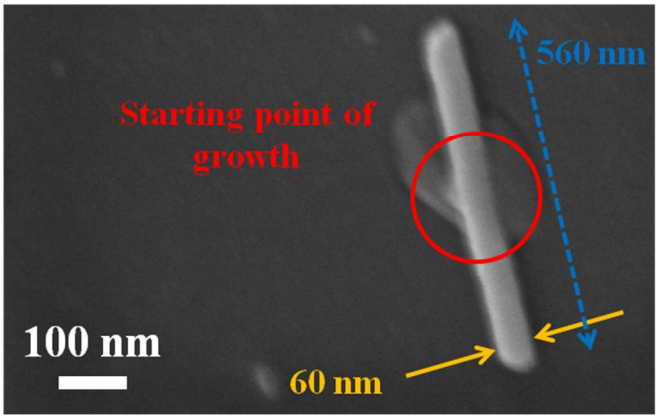

Fig. 5 Early stage of the NW growth from Au surface.

Next, an electron diffraction analysis was carried out to determine the direction of the NW growth. Figure 6(b) shows the diffraction pattern of the Fe NW shown in Fig. 6(a). There are two non-equivalent reciprocal spots, i.e., 200 and 112. The growth axis of the NW must be perpendicular to these two vectors ((200) and (112)), therefore, this diffraction pattern shows that the growth axis of the Fe NW was $[02\bar{1}]$. The electron diffraction pattern of the cross section of the Fe particle was also investigated and two non-equivalent reciprocal spots were assigned to 200 and 110 (see Fig. S4 in supplementary information). This result shows that the Fe NWs do not grow in the direction of [001] and the favourable growth axis of the Fe NWs is $[02\bar{1}]$. Combining the results of the XRD and electron diffraction (see below), the 200 peak in the XRD pattern originated from the Fe NWs and the other two peaks (110 and 112) in the XRD are mainly from the Fe particles.

Although the $[02\bar{1}]$ oriented growth was reported in Ref. 3, the mechanism has not been elucidated. It seems that the growth orientation of Fe NWs on $FeCl_2$ powder (Ref. 1 – 3) is determined by chance, yet we suspect it is determined by the epitaxial orientation of Fe-Au interface in the present experiment. In order to clarify this point, we made cross section of the Fe NWs and examined by TEM.

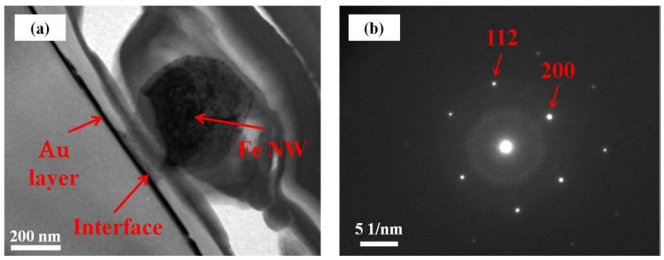

Fig. 6 (a) Cross-section TEM image of the Fe NW (b) electron diffraction pattern of the Fe NW shown in (a)

Furthermore, we noticed in the cross-section TEM image that the Au layer beneath the Fe NW is parallel to the (200) plane of the Fe NW as shown in Figs. 6(a) and (b) (i.e., (200) vector is perpendicular to the Au layer). This result strongly suggests that the epitaxial growth occurred during the first step of the Fe NW growth. To investigate the orientation of the Au surface after aggregation, Au nanoparticles were spin-coated on the M-plane Al_2O_3 substrate and annealed at 700 ºC for 30 min. Then an XRD analysis was carried out. The XRD pattern illustrates that some Au islands were oriented to (111) while other Au islands were oriented to (200) as shown in Fig. S5. Based on the calculated ratio of the lattice constants of Au (a_{Au}) and Fe (a_{Fe}), $a_{Au}/a_{Fe} = 0.408/0.286 = 1.426 \cong \sqrt{2}$ (lattice

mismatch is only 0.6%). Taking into account the crystal structures of α-Fe (bcc) and Au (fcc) and the lattice constants, Fe can epitaxially grow on Au 200[29-31]. These facts suggest that the epitaxial growth of Fe occurs on Au (100) during the first stage of the Fe NW growth. On the other hand, according to Ref. 32, γ-Fe (fcc) can be grown on Au (111) when the thickness is less than 1 nm. A phase transition from fcc to bcc occurs when thickness is greater than 1 nm, and the orientation of α-Fe is (110). In addition, Fe grown on Au (111) tends to have an island structure due to the large surface free energy of Fe and small surface free energy of Au. The results in Ref. 32 are consistent with the formation of the Fe particles and the 110 diffraction peak in the XRD.

The growth mechanism of the Fe NWs is schematically depicted in scheme 1. While the temperature of the furnace is being raised, the Au nanoparticles aggregate due to the strong affinity with the substrate and minimization of the surface energy. $FeCl_2$ is reduced to Fe by H_2 ($FeCl_2 + H_2 \rightarrow Fe + 2HCl$) on the surface of the Au islands. During the first stage of the reduction of $FeCl_2$, Fe is dissolved into the Au islands (solubility of Fe into Au at 700 ºC is 0.57%)[26]. Epitaxial growth occurs when the amount of dissolved Fe into Au had saturated. The NW growth starts in the direction of $[02\bar{1}]$ once the epitaxial growth occurs on the surface of the Au island. Only axial growth occurred while the NW was growing as seen in Figs. 4(b) and 5. The diameter of the NW grown for 5 min (60 nm: shown in Fig. 5) does not differ very much from that grown for 30 min (120 nm: shown in Fig. 4(b)), while the lengths of the NW grown 5 min and 30 min are 560 nm and 37.6 μm, respectively. This selective axial growth can be explained by the stability of the sidewall and Ehrlich-Schwoebel barrier of the Fe NWs[33]. In other words, Fe atoms would prefer to attach to the tip of the NW than the sidewall. Additionally, adatoms cannot overcome the potential barrier at the step edge in order to move from the tip to the sidewall. Although the most stable surface of α-Fe is (100)[34], some researchers have reported a theoretical prediction by the embedded atom method, which concluded some surfaces are stabilized due to the relaxation of atoms at the surface[35,36]. In particular, since the total relaxation (perpendicular and parallel movement of atoms) of the (112) surface of the first layer is the highest among the high index surfaces such as (112), (310), and (210), which show the tendency to become a more symmetric surface structure, the (112) surface would be relatively stable among the metastable surfaces[37]. Furthermore, there is the possibility that the (120) surface is more stable than the (100) surface in the H_2 atmosphere due to the surface adsorption.

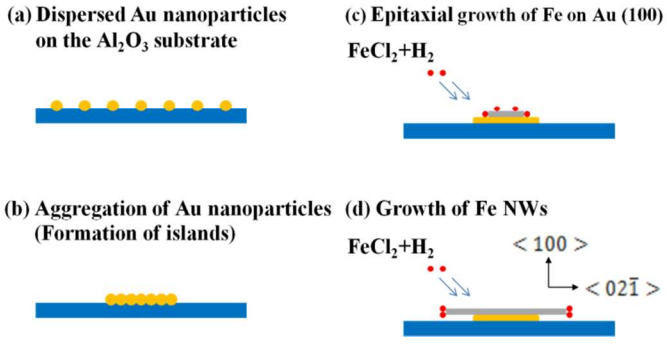

Scheme. 1 Growth mechanism of the Fe NW

Conclusions

We have fabricated Fe NWs on an Al_2O_3 substrate by CVD techniques. Separating the gas lines of H_2 and $FeCl_2$ vapour enabled us to continuously supply clean $FeCl_2$ vapour, which is crucial for the controlled and repeatable Fe NW growth. It was found that Au nanoparticles acted as catalysts and the morphology of the Fe NW strongly depended on the substrate. The M-plane Al_2O_3 was the best substrate to grow the Fe NWs with a high aspect ratio (approximately 300) During the first step of the NW growth, the Fe epitaxially grows on the surface of the Au islands with the orientation of (100). The epitaxial growth of Fe induces the NW growth, and the NWs grow horizontally to the substrate by a self-catalytic VS mechanism. The growth axis of the Fe NWs was determined to be $[02\bar{1}]$ based on the XRD and electron diffraction patterns.

Acknowledgements

T. Yanase received financial support from the MEXT (Japan) program "Strategic Molecular and Materials Chemistry through Innovative Coupling Reactions" of Hokkaido University.

A part of this work was conducted at "Joint-use Facilities: Laboratory of Nano-Micro Material Analysis", Hokkaido University, supported by "Nanotechnology Platform" Program of the Ministry of Education, Culture, Sports, Science and Technology (MEXT), Japan

Notes and references

[a] Frontier Chemistry Centre Faculty of Engineering, Hokkaido University, Kita-ku, Sapporo, Hokkaido 060-8628, Japan.
[b] Graduate School of Chemical Sciences and Engineering, Hokkaido University, Kita-ku, Sapporo Hokkaido 060-8682, Japan.
[c] Division of Materials Chemistry, Faculty of Engineering, Kita-ku, Sapporo, Hokkaido 060-8628, Japan.
[d] Graduate School of Engineering, Hokkaido University, Kita-ku, Sapporo, Hokkaido 060-8628, Japan.
[e] Creative Research Institution, Hokkaido University, Kita-ku, Sapporo, Hokkaido 060-8628, Japan.
[d] CREST, Japan Science and Technology Agency, Chiyoda-ku Tokyo 102-0076, Japan.

1 S. Kittaka and T. Kaneko, Japanese Journal of Applied Physics, 1969, **8**, 860.
2 T. Kaneko and Shigeyoshi Kittaka, Journal of Crystal Growth, 1977, **42**, 171.
3 R. N. Gardner, Journal of Crystal Growth, 1978, **43**, 425.
4 J. A. Salsgiver, IEEE Transactions on Magnetics, 1970, **6**, 741.
5 C. Cheze, L. Geelhaar, A. Trampert, O. Brandt and H. Riechert, Nano Letters, 2010, **10**, 3426.
6 K. T. Chan, J. J. Kan, C. Doran, L. Ouyang, D. J. Smith and E. E. Fullerton, Nano Letters, 2010, **10**, 5070.
7 L. Mohaddes-Ardabili, J. Zheng, S. B. Ogale, B. Hannoyer, W. Tian, J. Wang, S. E. Lofland, S. R.Shinde, T. Zhao, Y. Jia, L. Salamanca-Riba, D. G. Schlom, M. Wutting and R. Ramesh, Nature Materials, 2004, **3**, 533.
8 S. M. A. Shibli, K. S. Beenakumari, N. D. Suma, Biosensors and Bioelectronics, 2006, **22**,633.
9 S. Yang, H. Zhu, D. Yu, Z. Jin, S. Tang and Y. Du, Journal of Magnetism and Magnetic Materials, 2000, **222**, 97.

10 X. Wang, C. Li, G. Chen, C. Peng, L. He and L. Yang, Surface Review and Letters, 2010, **17**, 419.
11 Y. Peng, T. H. Shen, B. Ashworth, X. G. Zhao, C. A. Faunce and Y. W. Liu, Applied Physics Letters, 2003, **83**, 362.
12 W. Zhang, M. E. Bowden and K. M. Krishnan, Journal of Applied Physics, 2013, **113**, 17B502.
13 H. Pan, B. Liu, J. Yi, C. Poh, S. Lim, J. Ding, Y. Feng, C. H. A. Huan and J. Lin, Journal of Physical Chemistry B, 2005, **109**, 3094.
14 J. Goldberger, R. He, Y. Zhang, S. Lee, H. Yan, H. J. Choi and P. Yang, Nature, 2003, **422**, 599.
15 M. S. Gudiksen, L. J. Lauhon, J. Wang, D. C. Smith and C. M. Lieber, Nature, 2002, **415**, 617.
16 L. J. Lauhon, M. S. Gudiksen, D. Wang and C. M. Lieber, Nature, 2002, **420**, 57.
17 D. H. Kuo and B. J. Chang, Crystal Growth and Design, 2010, **10**, 977.
18 K. Ikejiri, F. Ishizaka, K. Tomioka and T. Fukui, Nanotechnology, 2013, **24**, 115304.
19 S. Hong, J. Yeo, W. Manorotkul, H. W. Kang, J. Lee, S. Han, Y. Rho, Y. D. Suh, H. J. Sung and S. H. Ko, Nanoscale, 2013, **5**, 3698.
20 J. P. Alper, A. Gutes, C. Carraro and R. Maboudian, Nanoscale, 2013, **5**, 4114.
21 K. T. Chan, C. Doran, E. G. Shipton and E. E. Fullerton, IEEE Transactions on Magnetics, 2010, **46**, 2209.
22 Y. Li, J. Li, K. Zhang and K. M. Liew, Carbon, 2012, **50**, 566.
23 M. A. Zeeshan, S. Pane, S. K. Youn, E. Pellicer, S. Schuerle, J. Sort, S. Fusco, A. M. Lindo, H. G. Park and B. J. Nelson, Advanced Functional Materials, 2013, **23**, 823.
24 W. Kern, Journal of Electrochemical Society, 1990, **137**, 1887.
25 G. Frens, Nature Physical Science, 1973, **241**, 20.
26 H. Okamoto, Physica B, 1988, **149**, 194.
27 R. S. Wagner and W. C. Ellis, Applied Physics Letters, 1964, **4**, 89.
28 K. H. Cho and Y. M. Sung, Nanoscale, 2013, **5**, 3690.
29 A. M. Begley, S. K. Kim, J. Quinn and F. Jona, Physical Review B, 1993, **48**, 1779.
30 S. D. Bader and E. R. Moog, Journal of Applied Physics, 1987, **61**, 3729.
31 S. D. Bader, E. R. Moog and P. Grunberg, Journal of Magnetism and Magnetic Materials, 1986, **53**, L295.
32 D. T. Dekadjevi and B. J. Hickey, Physical Review B, 2005, **71**, 054108.
33 D. J. Shu, X. Xiong, Z. W. Wang, Z. Zhang, M. Wang and N. B. Ming, Journal of Physical Chemistry C, 2011, **115**, 31.
34 G. Grochola, S. P. Russo, I. Yarovsky and I. K. Snook, Journal of Chemical Physics, 2004, **120**, 3425.
35 M. I. Haftel, T. D. Andreadis and J. V. Lill, Physical Review B, 1990, **42**, 11 540.
36 J. Sokolov and F. Jona, Physical Review B, 1985, **31**, 1929.
37 J. Sokolov and F. Jona, Solid State Communications, 1984, **49**, 307.